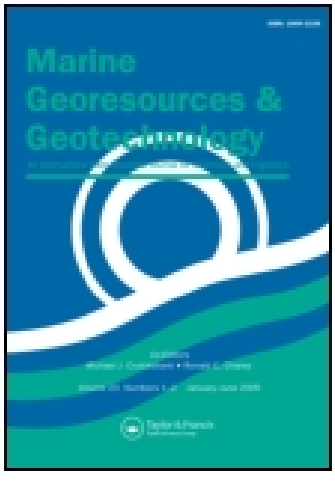

Marine Georesources & Geotechnology
Publication details, including instructions for authors and subscription information:
http://www.tandfonline.com/loi/umgt20

The performance of drag anchor and chain systems in cohesive soil

S. R. Neubecker [a b] & M. F. Randolph [a]
[a] Department of Civil Engineering , The University of Western Australia , Perth, Australia
[b] Geomechanics Group , The University of Western Australia , Nedlands, Western Australia, 6907, Australia
Published online: 23 Dec 2008.

To cite this article: S. R. Neubecker & M. F. Randolph (1996) The performance of drag anchor and chain systems in cohesive soil, Marine Georesources & Geotechnology, 14:2, 77-96, DOI: 10.1080/10641199609388305

To link to this article: http://dx.doi.org/10.1080/10641199609388305

The Performance of Drag Anchor and Chain Systems in Cohesive Soil

S. R. NEUBECKER
M. F. RANDOLPH

Department of Civil Engineering
The University of Western Australia
Perth, Australia

The synthesis of anchor equilibrium equations with recently derived chain equilibrium expressions enables calculations for anchor system capacity which account for the anchor–chain interaction. This forms the basis for a study into the effects of relative chain size on anchor performance, and extrapolation of scale-model tests to prototype events. Applications of these expressions are particularly suited to clay soils, where the failure mechanism of the soil is local and hence the anchor capacity is essentially independent of anchor orientation. Expressions are derived for the ultimate holding capacity of anchors in terms of two fundamental anchor parameters. Analytical relationships for the development of embedment and capacity with drag distance are shown to compare favorably with numerical solutions and also with field test data.

Keywords anchors, chain profile, drag anchor, efficiency, embedded anchor chain, scaling, ultimate holding capacity

As a drag anchor penetrates into soil, the resulting sliding and cutting forces on the anchor chain cause it to form an inverse catenary curve from the anchor to the soil surface as shown in Figure 1. Two important features are brought about by the behavior of the chain. First, the chain tension is reduced from the seabed to the anchor due to the frictional stresses between the chain and the soil. Second, the chain will be inclined to the horizontal at the anchor padeye, which in turn induces a vertical load on the anchor. The chain behavior is therefore an imperative consideration in the overall anchor system analysis.

The solution of the anchor chain profile and frictional capacity has traditionally involved numerical integration of the governing differential force equilibrium equations. Vivatrat et al. (1982) presented the tangential and normal force equilibrium equations of a chain element (illustrated in Figure 2) as

$$\frac{dT}{ds} = F + w \sin \theta \tag{1a}$$

$$T \frac{d\theta}{ds} = -Q + w \cos \theta \tag{1b}$$

where T is the tension in the chain, θ is the angle subtended by the chain to the horizontal, s is the distance measured along the chain starting at the attachment

Received 17 April 1995; accepted 23 August 1995.
Address correspondence to Dr. Steve Neubecker, The University of Western Australia, Geomechanics Group, Nedlands, Western Australia 6907, Australia.

Marine Georesources and Geotechnology, 14:77–96, 1996

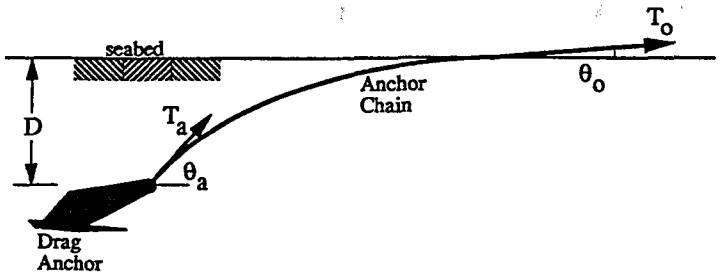

Figure 1. Anchor–chain system showing inverse catenary shape of chain.

point, F and Q are the tangential and normal forces per unit length of the chain, respectively, and w is the buoyant weight of the chain per unit length.

The solution incorporates an iterative scheme whereby, for a given chain tension, T_a, at the attachment point (at a known depth, D), a chain angle, θ_a, is first assumed. The equations are then integrated over the embedment depth to provide an estimate of the chain angle, θ_0, at the surface of the seabed. The attachment angle, θ_a, is then varied until the surface angle, θ_0, matches the required value (usually assumed to be zero).

Considerable computational effort is required to solve the chain characteristics this way, but more important, the numerical nature of the method has prevented a simplified analysis of the interactive effects between the anchor and the chain.

Neubecker and Randolph (1995) developed a simple expression that relates tension and inclination of the chain at a given padeye depth, in a soil with any strength profile, along with relationships that express frictional dissipation and chain profiles. The primary expressions that will be used in the ensuing analysis relate tension at the padeye and seabed to the inclination of the chain at these two points. For the typical case of $\theta_0 = 0$, the first expression, with relates T_a and θ_a, is

$$\frac{T_a \theta_a^2}{2} = D\bar{Q} \tag{2}$$

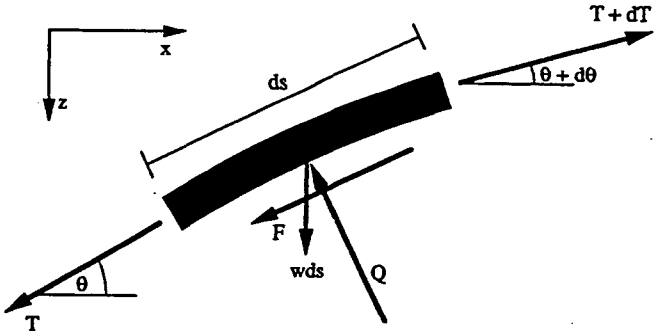

Figure 2. Force equilibrium of a chain element.

where $\overline{Q}$ is the average bearing resistance (force per unit length) of the chain in the soil. The expression for frictional development along the chain was derived as

$$\frac{T_0}{T_a} = e^{\mu\theta_a} \tag{3}$$

where μ is the friction coefficient between the chain and the soil. These equations provide simple functional relationships between key variables, and as such form the basis for much of the following analysis.

Simplifying Anchor Simulation Programs

Drag anchor simulation programs currently operate by incrementally advancing the anchor through the soil, assuming that it travels parallel to the flukes. At each step, the soil pressures acting on the various elements of the anchor are calculated using standard bearing capacity-type calculations. A new orientation of the anchor is also calculated by moment equilibrium considerations assuming centers of pressure for each of the soil reactions. An example of a system of soil reactions that may be used to model force and moment equilibrium of an anchor is shown in Figure 3. At each incremental advance of the anchor, the chain equations need to be solved to evaluate the chain inclination at the shackle (which affects moment equilibrium) and the chain tension at the mudline. This requires considerable computational effort, as already described.

The assumption that a drag anchor travels parallel to its flukes is widely accepted, and is supported by the observation that the anchor flukes typically reach a horizontal attitude at ultimate holding capacity (Dunnavant and Kwan, 1993). Therefore, in order to simplify the calculation method, it is rational to express the geotechnical resisting force acting on the anchor parallel to the direction of travel, T_p, as a product of the frontal projected area and the local bearing capacity of the soil, such as

$$T_p = fA_pN_cs_u \tag{4}$$

where A_p is the projected anchor area (in the direction of travel), N_c is a bearing capacity factor, s_u is the local undrained shear strength, and f is a form factor for the anchor. It is evident from moment equilibrium that for a weightless anchor there will be geotechnical forces normal to the fluke, T_n, such that the resultant

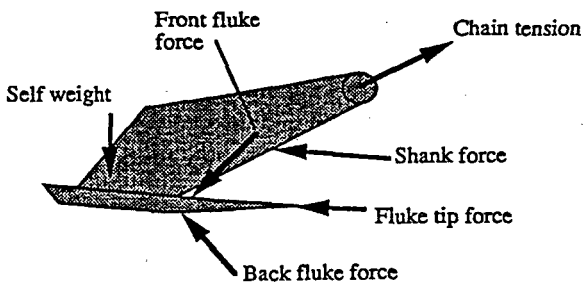

Figure 3. Example of a force system acting on a drag anchor.

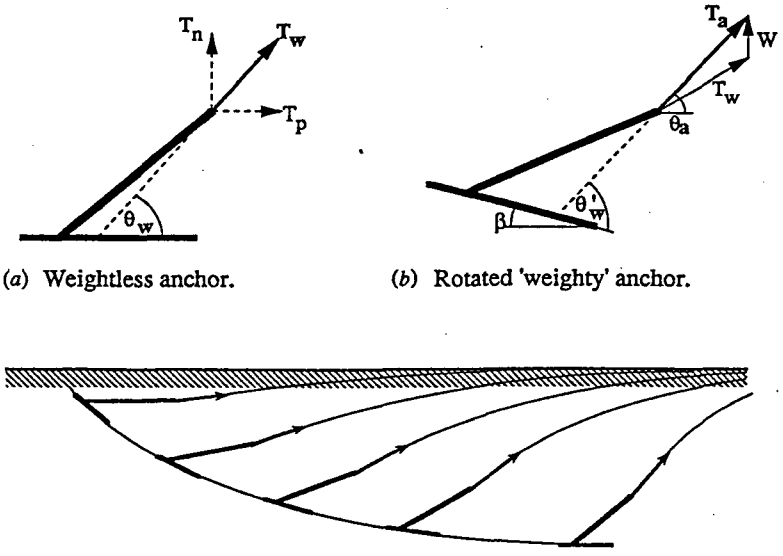

(*a*) Weightless anchor. (*b*) Rotated 'weighty' anchor.

(*c*) Anchor embedment.

Figure 4. Anchor resistances and embedment trajectories.

resisting force of the weightless anchor, T_w, will make a unique angle with the fluke, θ_w. Therefore, with reference to Figure 4*a*,

$$T_w = \frac{T_p}{\cos \theta_w} \tag{5}$$

The angle of the resultant to the fluke, θ_w, may be taken as a geometric characteristic of the anchor. There will be a minor variation in the value of θ_w due to differential soil strength over the depth occupied by the anchor. However, considering the deep embedment achieved by drag anchors in clay, this differential is assumed to be small and hence θ_w is taken as a constant.

During embedment, the anchor fluke will be at some angle, β, to the horizontal, and the anchor weight will lead to modified resistance components parallel and normal to the anchor fluke, and hence a modified resultant angle, θ'_w, as shown in Figure 4*b*. The chain angle at the padeye will be

$$\theta_a = \theta'_w - \beta \tag{6}$$

Simulation of anchor embedment may then proceed as follows:

1. From a given starting point (e.g., anchor shank horizontal, embedment depth zero), advance the anchor through a horizontal increment, Δx.
2. Calculate the new embedment depth, assuming motion parallel to the previous fluke orientation.
3. Calculate the anchor resistance, T_a, and its orientation relative to the anchor, θ'_w, from the anchor characteristics and local soil strength.
4. Calculate the chain angle, θ_a, using Eq. (2), taking account of the average chain resistance through the superficial soil.

5. Calculate the anchor tension at mudline, T_0, using Eq. (3).
6. Adjust the anchor angle, β, using Eq. (6) in order to satisfy equilibrium.
7. Increment the anchor displacement by a further Δx, and loop to step 2.

The anchor will follow a path as indicated in Figure 4*c*, where the anchor chain makes an almost constant angle to the fluke (the variation being due to the gradually lessening effect of the anchor weight, as the anchor embeds and capacity increases). Every anchor therefore can be considered to have inherent properties f and θ_w, which are unique to that anchor and are capable of describing the behavior of it in any cohesive soil profile. These anchor properties could be evaluated by: (1) experimental investigation, (2) calibration against field data, (3) results from analyses using the currently available drag anchor simulation programs, or (4) detailed analysis using a finite-element package.

Even though the above procedure is still an incremental simulation of the anchor embedment, it does have advantages over existing simulation programs. Primarily, the whole simulation can be run using a simple spreadsheet and the simulation is completed almost instantaneously, even for over 250 increments of anchor movement.

Figure 5 shows the results of the above analysis applied to a 15-t Stevpris anchor. The soil strength profile was $s_u = 1.26z$ kPa, where z is the depth in meters, and the effective chain diameter was 0.16 m; as such it was an analysis of a centrifuge test (test A) reported by Dunnavant and Kwan (1993). The projected anchor area was calculated to be $A_p = 7.0$ m^2 (including the opening between the twin shanks) and form factor $f = 1.3$, with a value of $\theta_w = 0.61$ radians (35°) and a bearing capacity factor $N_c = 9$. The results compare very well with the experimental ones in which the efficiency was 24 and dive depth was between 5 and 6 fluke lengths after a drag of 21 fluke lengths. It should also be noted that the general shape of the penetration and load curves also agree with the industry accepted behavior of drag anchors in clay.

The form factor, f, and characteristic θ_w adopted for the above analysis are not necessarily precise properties of the anchor, but should be taken as estimates which are consistent with the model results. It should be noted that other combinations of f and θ_w can produce similar results. For example, taking $f = 1$ and $\theta_w = 40°$ results in an efficiency of 23 and a dive depth of 6.7 fluke lengths,

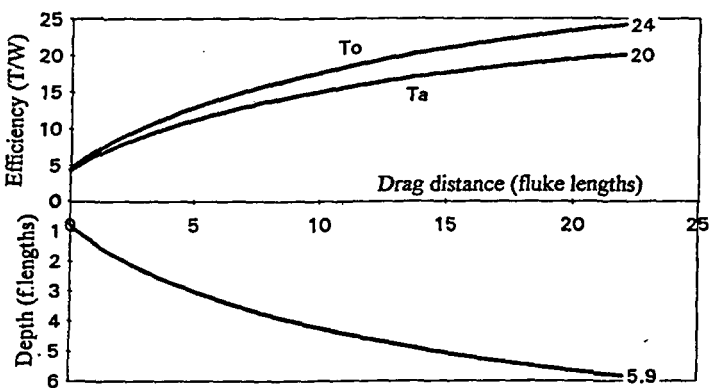

Figure 5. Load development and penetration curves for a 15-t Vryhof Stevpris.

which are also reasonably close to the reported measurements. Once appropriate values have been derived for the coefficients, f and θ_w, it becomes straightforward to predict the anchor response in any given soil profile.

Prediction of Maximum Embedment Depth

Assuming that the anchor always travels parallel to its fluke and at some angle, β, to the horizontal, it clearly follows that at the ultimate holding capacity (UHC) the anchor ceases to penetrate further and hence the angle $\beta = 0$. During embedment, when $\beta > 0$, it may be shown that (see Figure 6)

$$\theta_a \approx \theta_w - \beta + \frac{W\cos(\theta_w - \beta)}{T_w} \tag{7}$$

and also

$$T_a \approx T_w + W\sin(\theta_w - \beta) \tag{8}$$

It is convenient at this point to define anchor efficiencies η_w, η_a, and η_0 which are determined by normalizing the anchor capacities T_w, T_a, and T_0, respectively, by the submerged weight of the anchor, W. From Eq. (2), substitutions for T_a and θ_a can be made to give the following equilibrium relationship at UHC ($\beta = 0$):

$$T_w\left(1 + \frac{\sin\theta_w}{\eta_w}\right)\left(\theta_w + \frac{\cos\theta_w}{\eta_w}\right)^2 = 2D\bar{Q} \tag{9}$$

where

$$\eta_w = \frac{T_w}{W} \tag{10}$$

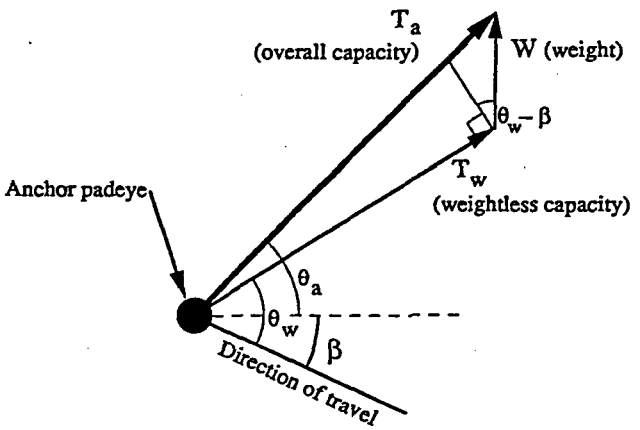

Figure 6. Force equilibrium of anchor.

For any cohesive soil strength profile, T_w can be written as

$$T_w = \frac{fA_p N_c s_u(z)}{\cos \theta_w} \tag{11}$$

and $D\overline{Q}$ can be written as

$$D\overline{Q} = bN_c \int_0^z s_u \, dz \tag{12}$$

where b is the effective width of the cable or chain. For cable, the effective width is simply the cable diameter, whereas in the case of chain the effective width can be taken as 2.5 times the nominal bar diameter of the chain (Degenkamp and Dutta, 1989). Substitution of both these terms into Eq. (9) and simplification produces

$$\frac{\int_0^{z_{UHC}} s_u \, dz}{s_u(z_{UHC})} = \frac{fA_p}{2b}\left(\frac{\theta_w^2}{\cos \theta_w} + \frac{2\theta_w + \theta_w^2 \tan \theta_w}{\eta_w}\right) \approx \frac{fA_p \theta_w}{2b \cos \theta_w}\left(\theta_w + \frac{2}{\eta_w}\right) \tag{13}$$

The simpler form of Equation (13) is valid for typical cases where θ_w is less then 1 rad. In many instances the soil strength profile is able to be described by the power law

$$s_u(z) = S_0\left(\frac{z}{z_0}\right)^{\alpha} \tag{14}$$

where S_0 is the shear strength at some reference depth z_0, with $\alpha = 1$ corresponding to soil with strength increasing linearly with depth and $\alpha = 0$ corresponding to uniform soil. When this is the case, Eq. (13) can be simplified to express z_{UHC} as

$$z_{UHC} = \frac{(\alpha + 1) fA_p \theta_w}{2b \cos \theta_w}\left(\theta_w + \frac{2}{\eta_w}\right) \tag{15}$$

Some iteration is needed in the solution because the final embedment depth is a function of the efficiency η_w, which is in turn a function of embedment depth. The solution proceeds by assuming a weightless efficiency η_w, then calculating z_{UHC} by Eq. (15), then substituting the shear strength at the ultimate embedment depth into Eq. (11) to calculate T_w, and hence using this to verify the initial assumed efficiency and refine the solution.

For more complex soil strength profiles that cannot be described by the power law in Eq. (14), it is necessary to consider the ratio of the integral of soil strength to local soil strength, as expressed on the left-hand side of Eq. (13). This is an important ratio because it allows the maximum embedment depth to be calculated for *any* cohesive soil strength profile. It is evident that the anchor will penetrate to a depth where the ratio of $\int s_u \, dz$ to $s_u(z)$ is more or less constant, with a small difference due to the iterations of η_w. Figures 7*a* and 7*b* show schematically how the presence of a stiff soil layer near the surface reduces the embedment depth by the requirement of maintaining a (near) constant $\int s_u \, dz$ to $s_u(z)$ ratio. Furthermore, the need for idealized soil strength profiles is eliminated, and Figure 7*c* shows how a complex soil profile obtained from a cone test could be used to calculate embedment depth.

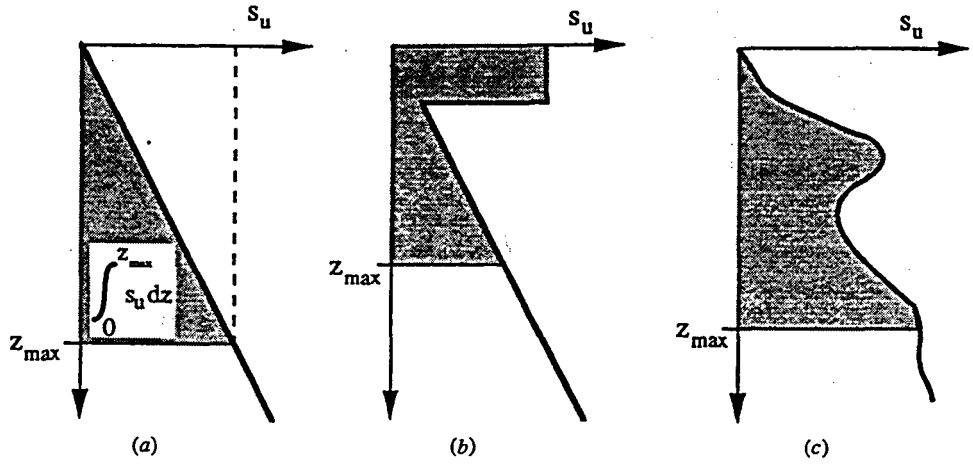

Figure 7. Ultimate embedment depth determined by soil strength profile for (*a*) simple profile; (*b*) stiff layer; (*c*) general profile.

Solution can proceed by standard iterative refinement of solutions or a graphical technique whereby the left- and right-hand sides of Eq. (13) are plotted against depth (note that η_w on the right-hand side needs to be replaced by the expansion of T_w/W so that both sides are a function of s_u and hence depth). In the graphical solution, the intersection of the two graphs will indicate the ultimate embedment depth of the anchor, and then the UHC follows easily from Eq. (11). Figure 8 shows how this technique can be applied to a complex soil profile.

Anchor Efficiency in Soil with Strength Proportional to Depth

For soil where the strength increases linearly with depth, the strength profile can be described by $s_u = kz$, where k is the soil strength gradient. From Eq. (11), the

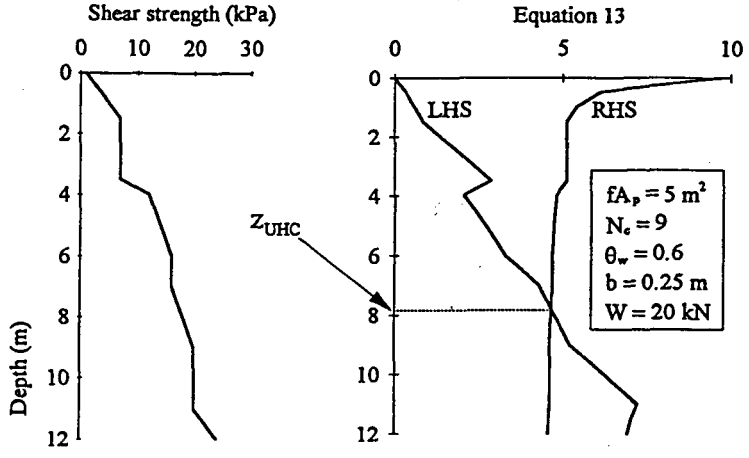

Figure 8. Graphical solution method to determine ultimate embedment depth.

weightless efficiency can be written as

$$\eta_w = \frac{T_w}{W} = \frac{fA_p N_c kz}{W \cos \theta_w} \tag{16}$$

Substitution of z_{UHC} from Eq. (15) ($\alpha = 1$) into this equation will yield the ultimate efficiency of the anchor, so that

$$\eta_w = \frac{fA_p N_c k}{W \cos \theta_w} \left(\frac{fA_p \theta_w}{b \cos \theta_w} \right) \left(\theta_w + \frac{2}{\eta_w} \right) \tag{17}$$

For simplification, the following nondimensional group can be defined:

$$\Pi_1 = \frac{(fA_p)^2 N_c k}{Wb} \tag{18}$$

Finally, it can be shown that for $\eta_w \gg 1$,

$$\eta_w = \Pi_1 \left(\frac{\theta_w}{\cos \theta_w} \right)^2 + \frac{2 \cos \theta_w}{\theta_w} \tag{19}$$

The form of this equation is confirmed by results published by Dunnavant and Kwan (1993). Along with extensive centrifuge testing of anchors in clay, a series of anchor simulations were performed using the program STA-Anchor. One of the results of the simulations was that a doubling of the soil strength gradient from 0.95 kPa/m to 1.9 kPa/m produced an increase in the anchor efficiency from 13 to 23.5 (an increase of 80%). This is consistent with the above equation, where doubling the nondimensional number Π_1 will result in an increase in the value of η_w of slightly less than 2. Even though the figures quoted by Dunnavant and Kwan (1993) refer to overall efficiencies η_0, the weightless efficiency, η_w, can be assumed to exhibit the same trends. It can be shown from Eq. (8) that

$$\eta_a \approx \eta_w + \sin \theta_w \tag{20}$$

Then, from Eq. (3),

$$\eta_0 \approx (\eta_w + \sin \theta_w) \exp \left[\mu \left(\theta_w + \frac{\cos \theta_w}{\eta_w} \right) \right] \tag{21}$$

A cautionary note needs to be made here about the concept of efficiency. In the preceding expressions, all of the efficiencies are obtained by normalizing a tension with the submerged weight of the anchor. It is traditional, however, to express anchor efficiency as a multiple of the dry weight of the anchor. The overall efficiency given in Eq. (21) therefore needs to be reduced by 13% (for a steel anchor with a specific gravity of 7.8) to convert from the submerged-weight efficiency to a conventional dry-weight efficiency.

Figures 9*a* and 9*b* show how weightless and overall efficiencies vary with nondimensional number Π_1 (for an assumed value of $\mu = 0.3$). Equation (19) is an extremely useful expression, as it allows an instant appraisal of the effect of the change of one variable on the resultant efficiency. For instance, a common practice in the industry to increase anchor holding power is to fill the hollow flukes of an

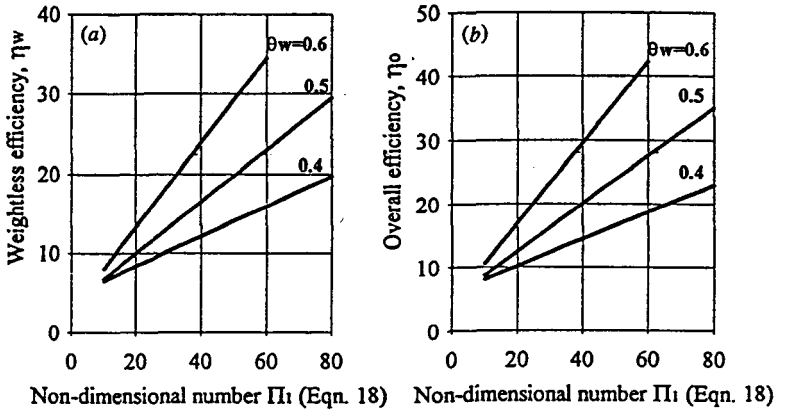

Figure 9. Anchor efficiencies in soil with linearly increasing strength with depth: (*a*) weightless efficiency; (*b*) overall efficiency.

anchor with some sort of ballast to increase the anchor weight. It can be shown here that an increase in anchor weight will result in a decrease of efficiency, but (by multiplying the equation through by W) the holding capacity can be shown to be slightly increased.

Anchor Efficiency in Uniform Soils

In a uniform soil the anchor efficiency can be written simply as

$$\eta_w = \frac{fA_p N_c s_u}{W \cos \theta_w} \tag{22}$$

since the soil strength does not change with depth. It is to be noted here that, with respect to the anchor characteristics θ_w and f, the efficiency is proportional to $f/\cos \theta_w$. In the case of soil with strength proportional to depth, the efficiency is approximately proportional to $(f\theta_w/\cos \theta_w)^2$. The important conclusion that can be drawn, therefore, is that some anchors will be more suitable for uniform soils and other anchors will be better suited to soils with linearly increasing strength.

To illustrate this point, consider anchor A, with θ_w and f parameters equal to 0.6 and 1.2, respectively, compared to anchor B, with identical weight and size but with θ_w and f parameters equal to 0.5 and 1.3. It can be seen that in a soil with linearly increasing strength, anchor A is preferred because it has the highest $(f\theta_w/\cos \theta_w)^2$ ratio. However, anchor B is preferred in a uniform soil because it has a higher $f/\cos \theta_w$ ratio. The ratios presented can be considered as a measure of suitability of an anchor to a certain soil profile, and therefore if accurate estimates of the characteristics θ_w and f can be made for a range of anchors, then the preceding argument could be used to ensure that the most efficient one is chosen.

A corollary of this conclusion is that very slight alterations could be made to an anchor to maximize its effectiveness in a given soil profile. Such alterations could be the omission of the small wings at the top of the shank of the anchor (as included on a Vryhof Stevpris), or the presence/absence of fluke stabilizers, or

changing the number of bracing bars between twin shanks. It is conceptually possible to alter the anchor characteristics to fine-tune its performance. However, these ideas are for consideration only and will not be developed further.

Prediction of Anchor Trajectory

For soils that obey the power law in Eq. (14), it is possible to develop a closed-form expression that approximates the trajectory of a drag anchor. First, it is necessary to consider a weightless anchor so that $\theta'_w = \theta_w$ and express Eq. (6) in the differential form

$$\frac{dz_w}{dx} \approx \beta = \theta_w - \theta_a \tag{23}$$

where z_w is the z coordinate of a weightless anchor. Substituting θ_a from Eq. (2) gives

$$\frac{dz_w}{dx} \cong \theta_w - \sqrt{\frac{2b \cos \theta_w z_w}{(\alpha + 1) f A_p}} \tag{24}$$

The solution of this equation is

$$x = \frac{-2}{C^2}\left[C\sqrt{z_w} + \theta_w \ln\left(1 - \frac{C}{\theta_w}\sqrt{z_w}\right)\right] \tag{25}$$

where

$$C = \sqrt{\frac{2b \cos \theta_w}{(\alpha + 1) f A_p}} \tag{26}$$

It is evident that the maximum penetration depth will be $(\theta_w/C)^2$, which agrees with Eq. (15), where $\eta_w = \infty$, as is appropriate for a weightless anchor. This penetration depth is obviously less than the depth attained by a weighty anchor, so it is necessary to correct the z coordinate to account for the anchor self-weight. This is done somewhat empirically by transforming the weightless z coordinate, z_w, to an actual coordinate, z_a, by

$$\frac{z_w}{(\theta_w/C)^2} = \left(\frac{z_a}{z_{\text{UHC}}}\right)^i \tag{27}$$

This transformation has the effect of forcing the maximum embedment depth to become z_{UHC} rather than the lesser value of $(\theta_w/C)^2$, as calculated for the weightless case. If the value of the index, i, is chosen to be 1, then the transformation will be a simple linear scaling, or a stretching of the drag anchor trajectory. This transformation is considered to be appropriate for a uniform soil ($\alpha = 0$), because the importance of the self-weight is the same throughout the embedment. For soil with strength proportional to depth the index i is required to be greater than 1, because the self-weight is a more important factor in the early embedment stages.

The other main factor that affects the value of the index i is the anchor efficiency, η_w. A large anchor efficiency implies that there is little emphasis of the self-weight on the anchor behavior, and hence the index should be close to unity. With these factors in mind, a functional form of the index was derived empirically as

$$i = 1 + \frac{2\alpha^2}{\sqrt{\eta_w}} \tag{28}$$

After substituting the weight transformation equation into the weightless trajectory given in Eq. (25), the actual drag anchor trajectory becomes

$$x = \frac{-2\theta_w}{C^2}\left\{\left(\frac{z_a}{z_{UHC}}\right)^{i/2} + \ln\left[1 - \left(\frac{z_a}{z_{UHC}}\right)^{i/2}\right]\right\} \tag{29}$$

Further simplification of this drag anchor trajectory expression can be made by substituting C from Eq. (26), then normalizing with z_{UHC} from Eq. (15) to give

$$\frac{x}{z_{UHC}} = \frac{-2\eta_w}{\eta_w\theta_w + 2}\left\{\left(\frac{z_a}{z_{UHC}}\right)^{i/2} + \ln\left[1 - \left(\frac{z_a}{z_{UHC}}\right)^{i/2}\right]\right\} \tag{30}$$

It is also instructive to determine the inclination of the direction of anchor travel, β, for determining anchor equilibrium at a preultimate stage. It can be shown that

$$\tan\beta = \frac{dz}{dx} = \frac{\eta_w\theta_w + 2}{\eta_w i}\left[\left(\frac{z_a}{z_{UHC}}\right)^{1-i} - \left(\frac{z_a}{z_{UHC}}\right)^{1-(i/2)}\right] \tag{31}$$

Figures 10*a* and 10*b* show plots of the closed-form trajectory (both weightless and transformed) against the trajectory obtained from the simulation method described previously. For both examples the anchor has properties of $\eta_w = 20$ and $\theta_w = 0.6$. It is evident that the method of transforming the z coordinate to allow for self-weight results in a sufficiently accurate estimation of the drag anchor trajectory, despite the empirical nature of the weight correction.

It can be seen from Eq. (30) that the shape of the drag anchor trajectory is dependent only on α (from the index, i), η_w, and θ_w. A study of the sensitivity of each of these variables on the trajectory profile is made in Figures 11*a*, 11*b*, and 11*c*. It can be seen from these figures that the anchor trajectory is not very sensitive to any of the variables, and an embedment ratio of 90% corresponds fairly consistently to a drag ratio of about 5. This compares well to empirical observations (Vryhof Anchors, 1990) that drag anchors in clay typically reach their ultimate embedment depth of about 5 fluke lengths after a drag distance of 20 to 25 fluke lengths (hence a drag ratio of 4 to 5).

It should be noted here that the anchor theoretically never reaches its maximum embedment depth; rather it approaches a maximum embedment depth asymptotically. This suggests that for the estimation of drag distance to achieve a certain load, the embedment ratio must be calculated. More important, however, is the fact that the maximum design load must be significantly less than the UHC,

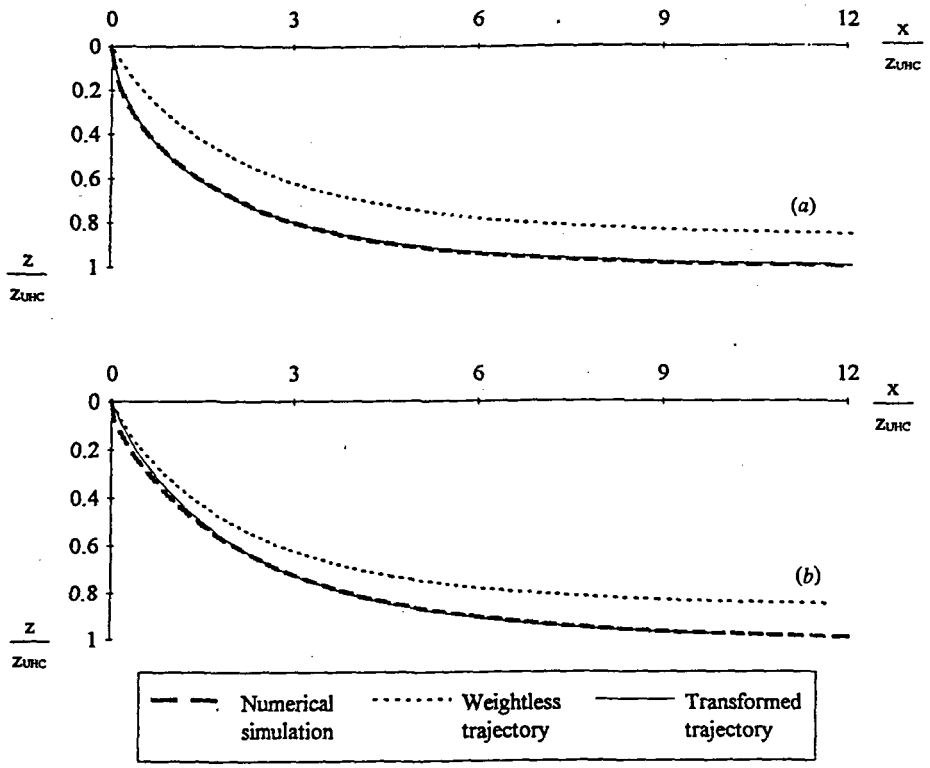

Figure 10. Comparison of closed-form anchor trajectories with numerical simulations for (*a*) $\alpha = 1$, and (*b*) $\alpha = 0$.

since the UHC is never reached. The penetration ratio and the capacity ratio are related by

$$\frac{T_{\max}}{T_{\mathrm{UHC}}} = \left(\frac{z_{\max}}{z_{\mathrm{UHC}}}\right)^{\alpha} \tag{32}$$

It can be seen that an anchor must be chosen to satisfy two conditions. First, T_{UHC} must be greater than the design load $T_{\max}$; and second, the ratio of $z_{\max}$ to z_{UHC} must be such that the drag distance to achieve the load is not excessive. An example of excessive dragging of the anchor would occur if a capacity ratio ($T_{\max}/T_{\mathrm{UHC}}$) of 98% was used in a soil with linearly increasing strength ($\alpha = 1$). From Eq. (32), a penetration ratio ($z_{\max}/z_{\mathrm{UHC}}$) of 98% is required, which brings about a drag distance that is two times greater than the drag distance required to attain a penetration ratio of 87%. In a case like this it may be well worth increasing the anchor size, hence decreasing the penetration ratio, in order to decrease the drag length required.

The problems associated with excessive drag lengths include longer installation times (and hence greater expense), greater difficulty in attaining the design capacity while the anchor is in the target area, the need to use longer chains than necessary in some cases, and greater chance of anchor instability. A trade-off between anchor size and drag distance needs to be made and is warranted in some

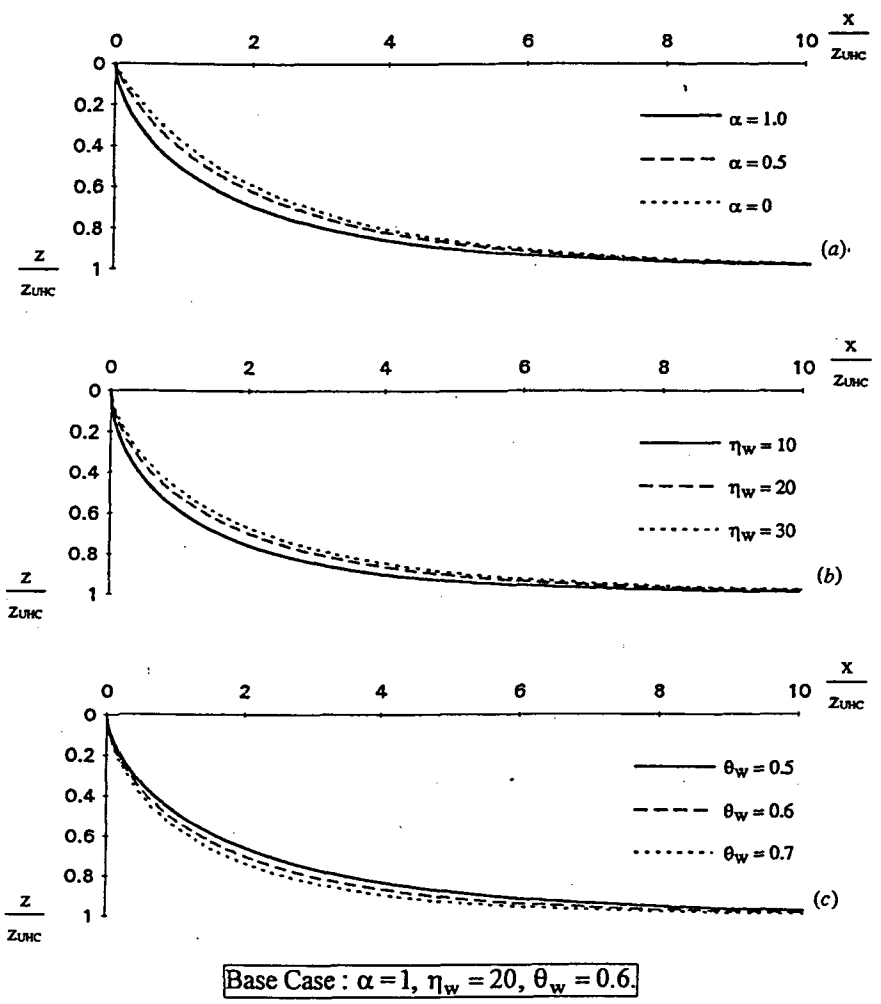

Figure 11. Sensitivity study of anchor trajectory to: (*a*) soil parameter α; (*b*) weightless efficiency η_w; (*c*) anchor parameter θ_w.

cases (such as the previous example), because a small increase in anchor size can correspond to a large decrease in drag distance.

Scaling Relationships for Drag Anchors

A further application of the chain solutions is in the assessment of how anchor capacity should scale with the size of the anchor. Most anchor design charts are based on extrapolation of the holding capacity of small anchors, using a power law of the form

$$T_{ult} = T_1 \left(\frac{W}{W_1} \right)^n \tag{33}$$

The exponent, n, expresses a reduction in anchor efficiency with anchor size, and arises due to a natural scaling dissimilarity between the anchor and the chain (Craig, 1994). The value of n is generally taken to lie in the range of $\frac{2}{3}$ to unity, with a value of 0.92 proposed by the U.S. Naval Civil Engineering Laboratory (NCEL, 1987b) for most commercially available anchors in soft soil.

A theoretical basis for determining the value of the exponent, n, can be developed by consideration of the chain tension and its compatibility with both anchor and chain conditions. In the following arguments a general soil profile that obeys the power law in Eq. (14) will be assumed.

Considering the anchor compatibility first, and by taking A_p proportional to the square of the anchor dimensions, and hence proportional to the $\frac{2}{3}$ power of the anchor weight, it is possible from Eq. (11) to write

$$T_a \propto D^{\alpha} W^{2/3} \tag{34}$$

(Note that, for simplicity, the anchor weight has been ignored in comparison to the ultimate capacity, hence $T_a \approx T_w$.)

Now, for compatibility of the chain tension with the chain, it is possible from Eq. (2) to write:

$$T_a \propto D\overline{Q} \propto bD^{1+\alpha} \tag{35}$$

(since $\overline{Q}$ is proportional to the average soil strength and the effective chain width, b). The depth of embedment may be eliminated from these two equations, to give an anchor capacity of

$$T_a \propto b^{-\alpha} W^{2(1+\alpha)/3} \tag{36}$$

The above arguments show that there is a theoretical basis for the manner in which anchor holding capacity varies with anchor and chain size in any given type of soil, and furthermore, the power law relationship depends on how the chain size varies with anchor size. Equation (36) can be extremely useful when extrapolating the results of tests on small anchors, as it takes into account the size of the chain (or wire rope) used in the model experiments. However, this equation is most useful when one considers that the chain dimension will always be *rounded up* to the nearest commercially available chain size, so that in reality the chain size will never be optimally scaled to the anchor. This equation allows for an extrapolation which is designed specifically for the particular anchor and chain sizes at the model and prototype scales.

The tensile capacity of the chain depends on the square of the diameter, and hence, if the assumption is made that the anchor efficiency is constant (i.e., T_a is proportional to W), then the chain size must increase in proportion to the square root of the anchor weight, which gives

$$T_a \propto W^{(4+\alpha)/6} \tag{37}$$

For soil where the strength is proportional to depth ($\alpha = 1$), the exponent n is equal to 0.83, while for soil with uniform strength ($\alpha = 0$), the exponent is 0.67.

The exponent may be increased marginally by allowing for the reduction in anchor efficiency with increasing anchor weight. By taking the chain diameter

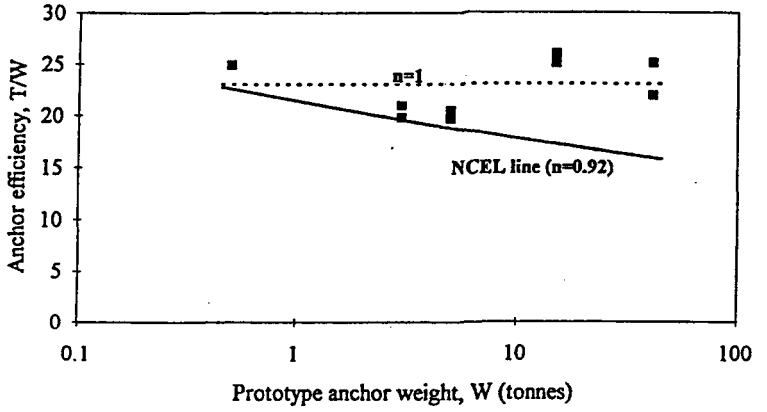

Figure 12. Efficiency versus anchor weight with experimental data from Dunnavant and Kwan.

proportional to the square root of the anchor holding capacity, it may be shown that the exponent, n, becomes

$$n = \frac{4(1 + \alpha)}{3(2 + \alpha)} \tag{38}$$

Now, for soil with strength proportional to depth, the upper limit of the exponent is 0.89. It can be seen that this value is very close to the empirically derived value of 0.92 proposed by NCEL (1987b) and suggests that this anchor–chain scaling effect is the sole cause of the decrease in anchor efficiency with size. More important, it highlights the inadequacies of the current design charts in which the exponent n is totally independent of soil profile.

Results from centrifuge modeling of drag anchors in clay have been presented by Dunnavant and Kwan (1993). Their experimental work consisted of testing the same model anchor and chain at different g levels to simulate prototype anchors of different sizes (from 0.5 to 45 t). A major limitation of this method for investigating potential scale effects is that the chain was not scaled correctly with prototype anchor size. Since the chain diameter was maintained in proportion to the anchor length, it will be progressively oversized (in terms of its tensile capacity) as the g level decreases (i.e., for the smaller prototypes).

The chain diameter was proportional to the anchor size in the centrifuge tests, or to the cube root of the weight,

$$b \propto W^{1/3} \tag{39}$$

Substitution of this into Eq. (36) with $\alpha = 1$ gives $T_a \propto W$, or in other words the exponent $n = 1$, which is to be expected because there is geometric similarity among all tests. Figure 12 shows the results of these tests on a log-linear plot rather than the standard log-log plot, which tends to mask discrepancies at the upper end. Even though there is significant scatter, it can be seen that the line $n = 1$ gives a better fit to the data than the NCEL line ($n = 0.92$). Again, therefore, the results emphasize the important influence of the chain diameter in determining the variation of anchor efficiency with anchor size.

Comparison with Published Drag Anchor Data

Published drag anchor test data are very limited, and much of the available data are rudimentary in that they contain little information about the soil conditions, anchor trajectory, and final penetration depth of the anchor. The U.S. Naval Civil Engineering Laboratory, however, has published anchor test data in both sand and clay (e.g., NCEL, 1980; Taylor, 1980), where extensive instrumentation of the anchor has resulted in a comprehensive set of anchor performance data.

A series of tests of several STATO-type anchors of different size were reported by Taylor (1980). STATO anchors with weights of 0.46 t, 1.36 t, and 3.0 t were tested in Indian Island mud, which is a normally consolidated silty clay with an undrained shear strength gradient of 1.62 kPa/m. A 51-mm nominal chain diameter was used for all tests, suggesting that anchor efficiency will actually increase with anchor size, as the chain becomes smaller with respect to the anchor. The data collected during each anchor test included drag distance, penetration, rotation (both longitudinal and transverse), and chain tension at the padeye, with the exception that no load data were recorded for the 3.0-t anchor.

To make a comparison between the test results and analytical results presented in this article, it is necessary to assume values for the anchor characteristics θ_w and f. These values were estimated to be 0.44 and 1.55, respectively, in order to give results consistent with the test data. The frontal projected area, A_p, of the 1.36-t anchor was estimated as 1.7 m^2 and was assumed to vary by anchor weight to the power of $\frac{2}{3}$. The analytical results are shown in Table 1, where the weightless efficiency was first calculated from Eq. (19) and then used in Eq. (15) to calculate the ultimate embedment depth, z_{UHC}.

Having determined the ultimate embedment depth, the trajectory is calculated directly from Eq. (30). The weightless capacity during embedment, T_w, follows easily from Eq. (11), which is then converted to an actual capacity, T_a, by Eq. (8). The load curve and trajectory comparisons are shown in Figure 13, and it can be seen that there is very good agreement between the field drag and the analytical results for all anchor sizes considered.

A further comparison can be made between the analytical results and a design curve for a NAVMOOR anchor published by the NCEL (1987a). Figure 14 presents the NCEL design curve for the embedment trajectory against Eq. (30) with $\alpha = 1$, $\theta_w = 0.5$, and $\eta_w = 20$. It is noted that the NCEL curve is a mapping of the fluke tip path, whereas the analysis is one of the anchor padeye. Nevertheless, excellent agreement is shown when the trajectories are normalized against their respective maximum penetration values. It is also implied in the NCEL design

Table 1
Analytical results

Anchor weight (t)	Projected area, A_p (m^2)	Weightless efficiency, η_w	Ultimate depth, z_{UHC} (m)
0.46	0.8	15.4	2.8
1.36	1.7	20.1	5.5
3.00	2.9	25.4	9.0

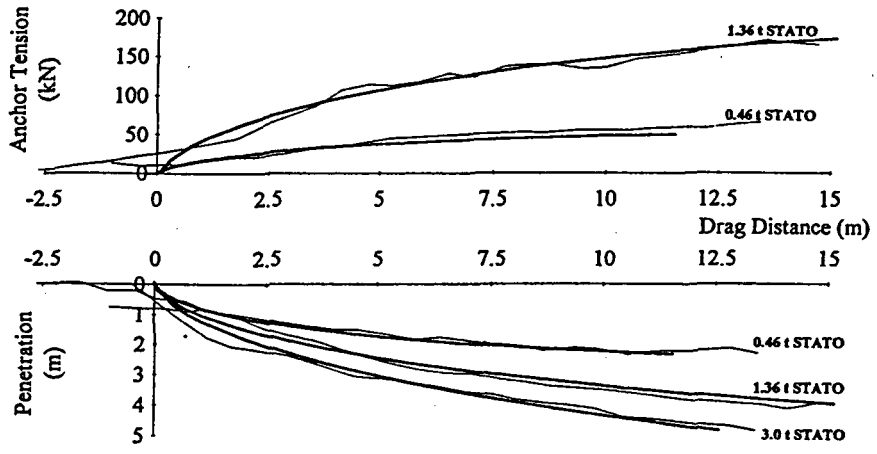

Figure 13. Comparison of analytical solution with NCEL data.

curve that anchor load is proportional to embedment depth. However, this is appropriate only for a normally consolidated clay with $\alpha = 1$.

Conclusions

Typically, drag anchor moorings are designed by the selection of the drag anchor type and size alone. Little consideration is currently given to the effect of the chain on the anchor system, and certainly no incorporation of the interative effects that exist between the anchor and the chain.

It has been demonstrated that the anchor chain plays a vital role in the overall system behavior of a drag anchor and chain mooring. Closed-form solutions for the ultimate embedment depth of a drag anchor have been developed which include chain effects, and are applicable in cohesive soils of any strength profile. In addition, expressions have been derived for the ultimate efficiency of a drag anchor in a cohesive soil with a simple strength profile, enabling an instant comparison of

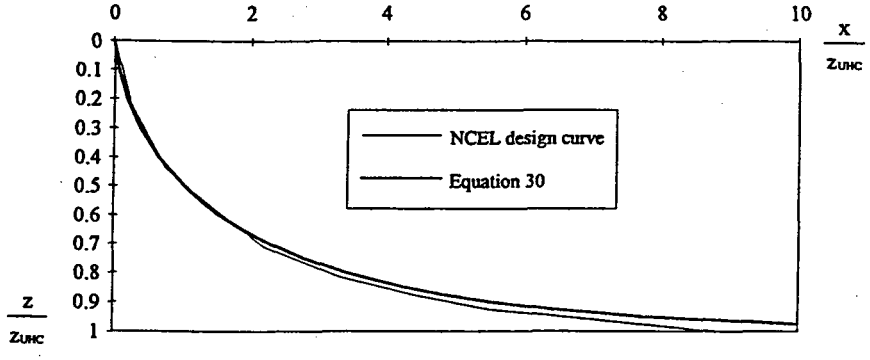

Figure 14. Comparison of analytical trajectory with NCEL design curve for a NAVMOOR anchor.

anchor types to determine which is most suited to a particular soil strength profile. Simple solutions have also been developed for calculation of the trajectory of drag anchors, which should prove invaluable for estimating the drag distance required to achieve a given load.

An interesting characteristic of the anchor–chain interaction occurs when the scaling similarity between these two components is considered. Larger anchors naturally require chains which are disproportionately larger than those of smaller anchors. This has the effect of a reduction in anchor efficiency with anchor size, which is well documented via empirical design charts. Expressions have been developed in this article which quantify this variation in efficiency with anchor size and are of considerable use when utilising small scale-model tests to interpret prototype anchor behavior.

In summary, the importance of taking due consideration of the chain when specifying an anchor–chain mooring is emphasized. The analytical expressions developed in this article provide a simple means for quantifying the interactive anchor–chain effects and, despite some idealizations in their development, have been shown to give excellent agreement with published data.

Nomenclature

A_p	projected anchor area
b	effective chain width
D	depth of chain attachment point
f	form factor for anchor resistance
F	tangential force per unit length of chain
k	gradient of Q with depth
N_c	bearing capacity factor
n	exponent for anchor efficiency
Q	normal force per unit length of chain
s	distance along chain
s_u	undrained shear strength of soil
S_0	shear strength at a depth of z_0
T	chain tension
T_n	anchor resistance normal to fluke
T_p	anchor resistance parallel to fluke
w	submerged chain weight per unit length
W	submerged anchor weight
x	horizontal distance
z	depth
z_{UHC}	depth at ultimate holding capacity
z_1	reference depth
α	soil strength profile exponent
β	inclination of anchor travel direction
η	anchor efficiency
θ	chain inclination from horizontal
θ_w	inclination of geotechnical anchor force to direction of travel
θ'_w	intrinsic chain inclination to direction of travel

μ chain–soil friction coefficient
Π_1 nondimensional group

Subscripts

a at the anchor
w weightless
0 at the soil surface

References

Craig, W. H. 1994. Size effects in anchor performance. *Canadian Geotechnical Journal* 31:450–454.

Degenkamp, G., and A. Dutta. 1989. Soil resistances to embedded anchor chains in soft clay. *Journal of the Geotechnical Engineering Division, ASCF* 115(10):1420–1438.

Dunnavant, T. W., and C-T. T. Kwan. 1993. Centrifuge modelling and parametric analyses of drag anchor behavior. *Proc., 25th Annual Offshore Technology Conference,* Houston, Texas, Paper 7202, pp. 29–39.

Naval Civil Engineering Laboratory. 1980. *Test data summary for commercially available drag embedment anchors.* U.S. Navy, Port Hueneme, CA.

Naval Civil Engineering Laboratory, 1987a. *The NAVMOOR anchor.* Techdata Sheet 87-05. U.S. Navy, Port Hueneme, CA.

Naval Civil Engineering Laboratory. 1987b. *Drag embedment anchors for navy moorings.* Techdata Sheet 83-08R. U.S. Navy, Port Hueneme, CA.

Neubecker, S. R., and M. F. Randolph. 1995. Profile and frictional capacity of embedded anchor chain. *Journal of the Geotechnical Engineering Division, ASCE* 121(11):797–803.

Taylor, R. J. 1980. *Conventional anchor test results at San Diego and Indian Island.* TN-1581, U.S. Naval Civil Engineering Laboratory, Port Hueneme, CA.

Vivatrat, V., P. J. Valent, and A. A. Ponterio. 1982. The influence of chain friction on anchor pile design. *Proc., 14th Annual Offshore Technology Conference,* Houston, Texas, Paper 4178, pp. 153–163.

Vryhof Anchors. 1990. *Anchor Manual.* Krimpen ad Yssel, The Netherlands.